

Designed Metamagnetism in $\text{CoMnGe}_{1-x}\text{P}_x$

Z. Gercsi,¹ K. Hono,² and K.G. Sandeman¹

¹*Dept. of Physics, Blackett Laboratory, Imperial College London, London SW7 2AZ UK*

²*Magnetic Materials Center, National Institute for Materials Science (NIMS), 1-2-1 Sengen, Tsukuba 305-0047, Japan*

We extend our previous theoretical study of Mn-based orthorhombic metamagnets to those that possess large nearest neighbour Mn-Mn separations ($d_1 \gtrsim 3.22 \text{ \AA}$). Based on our calculations, we design and synthesize a series of alloys, $\text{CoMnGe}_{1-x}\text{P}_x$, to experimentally demonstrate the validity of the model. Unusually, we predict and prepare several metamagnets from two ferromagnetic end-members, thus demonstrating a new example of how to vary crystal structure, within the $Pnma$ symmetry group, to provide highly tunable metamagnetism.

PACS numbers: 75.30.Sg, 75.30.Kz, 75.80.+q, 75.30.Et

I. INTRODUCTION

Manganese-based orthorhombic ($Pnma$) binary and ternary alloys are of fundamental research interest as they often exhibit complex, non-collinear magnetic structures that can be tuned by temperature, pressure and applied magnetic field. Some well-known examples are the set of fan, helical and cycloidal spin structures found in the (H, T) phase diagram of MnP^{1-3} , the cycloidal antiferromagnetism (AFM) of IrMnSi^4 and helical metamagnetism of $\text{CoMnSi}^{3,5}$. Various theoretical explanations have previously been suggested to describe the mechanisms responsible for the noncollinear magnetism of such materials. Some refer to competing symmetric and asymmetric exchange interactions^{2,6}; others to conduction-mediated indirect (RKKY) exchange⁷. Another potential cause put forward is band crossing and appropriate Fermi surface topology (nesting)^{4,8}.

One of the most feature-rich materials of this kind is CoMnSi on account of its pronounced magnetic field-induced tricritical metamagnetism and associated negative magnetocaloric effect (MCE)⁹. Our recent high-resolution neutron diffraction (HRPD) study¹⁰ uncovered a giant magneto-elastic coupling within the antiferromagnetic ground state of this system. It occurs as a change of up to 2% in nearest-neighbour Mn-Mn separations d_1, d_2 on heating. The field-induced tricriticality of this system can thus be understood as the result of tuning the metamagnetic critical temperature with an applied magnetic field to the point at which it coincides with this native giant magneto-elasticity.

Using Density Functional Theory (DFT) we recently examined the importance of the same Mn-Mn separations in determining the occurrence of different magnetic groundstates across several Mn-based orthorhombic ($Pnma$) systems¹¹. By applying hydrostatic expansion and compression to a prototype model MnP alloy, we found a stability criterion for the appearance of an AFM groundstate, rather than the usual FM state seen in MnP . This direct relation between Mn-Mn separation and magnetic groundstate can explain the energetic proximity of FM and AFM states in materials such as $\text{CoMnSi}^{3,5}$, $\text{MnAs}_{1-x}\text{P}_x$ ¹², $(\text{Fe}_{1-x}\text{Co}_x)\text{MnP}^{13}$

and $\text{NiMnGe}_{1-x}\text{Si}_x$ ¹⁴ where the nearest-neighbour Mn-Mn distances are close to a critical separation of $2.95 \text{ \AA} \lesssim d_1 \lesssim 3.05 \text{ \AA}$.

Although the latter model was computed in a large interval of $2.5 \text{ \AA} \lesssim d_1 \lesssim 3.22 \text{ \AA}$ to cover many of the relevant compositions in the literature, it may lead to a misinterpretation of a technologically relevant alloy with a larger $d_1 = 3.4 \text{ \AA}$ spacing: CoMnGe . CoMnGe is a collinear ferromagnet with a tendency to form a metastable hexagonal structure upon rapid cooling¹⁵. In this Article, we extend our previous theoretical analysis¹¹ towards larger Mn-Mn separations to explain the re-appearance of ferromagnetism in alloys with $d_1 \gtrsim 3.37 \text{ \AA}$. The importance of the correct theoretical description of latter composition is due its large magnetocaloric effect around room temperature¹⁶⁻¹⁸.

In this Article we first show the striking re-appearance of a FM groundstate at large interatomic Mn separations in Mn-based $Pnma$ alloys where $d_1 \gtrsim 3.37 \text{ \AA}$, thereby accounting for the magnetic properties of CoMnGe . Secondly, and significantly, we have designed a new alloy series, CoMn(P,Ge) based on our extended model in order to test and demonstrate its validity and in particular the dominance of the (d_1) Mn-Mn separation in determining the magnetic groundstate of the series of Mn-containing $Pnma$ alloys. We show that metamagnetism can be derived, unusually, by inter-doping two ferromagnetic end-compositions in order to bring d_1 to the critical regime where antiferromagnetism and ferromagnetism are similar in energy.

The remainder of the Article is organised as follows: first in Sec. II, the theoretical results calculated by applying DFT to the prototype MnP alloy are given. Based on this model, we present the structural and metamagnetic properties of purposefully designed $\text{CoMnGe}_{1-x}\text{P}_x$ alloys in Sec. III. Finally, a summary is made and conclusions are drawn in Sec. IV.

II. THEORETICAL

In our previous work we considered what we term the “prototype” binary MnP ($Pnma$) alloy and calculated

the effect of isotropic lattice expansion and compression on hypothetical non-magnetic (NM), ferromagnetic (FM) and antiferromagnetic (AFM) states by using the general gradient approximation method (GGA-DFT) implemented in VASP Kresse and Furthmüller¹⁹. We found the critical lattice parameters where a crossover from one magnetic state to another can occur¹¹. In that study, a single unit cell consisting of 8 atoms (4 Mn and 4 P) was used, which allowed three different collinear antiferromagnetic configurations (AFM1, AFM2 and AFM3) and a collinear ferromagnetic (FM) one to be constructed. In the interval of $2.5 \text{ \AA} \lesssim d_1 \lesssim 3.22 \text{ \AA}$ we were able to predict a transition in the zero temperature magnetic structure from NM to FM, and finally to AFM as a function of expanding lattice parameters. A detailed description of the DFT calculations is given in that work¹¹. Here we extend our simple binary model to $d_1 > 3.22 \text{ \AA}$ values by further hydrostatic expansion in order to interpret ferromagnetism in CoMnGe where $d_1 = 3.4 \text{ \AA}$ in the current model.

Fig. 1 shows the difference in energy between the possible collinear AFM and FM magnetic states ($\Delta E_{Tot} = E_{AFM} - E_{FM}$) as a function of Mn-Mn separation. Using this comparison scheme a non-FM state becomes most favourable when it has the most negative value of ΔE_{Tot} . On the left hand side of Fig. 1, the large compression causes a strong overlap of d -orbitals, and the broad d - d hybrid bands thus formed cannot support spontaneous magnetisation. In agreement with experimental findings, the FM state is the groundstate of MnP and is stable for intermediate deformations of the lattice. On further expansion of the lattice parameters, first the AFM1 type magnetic structure (at around $d_1 \sim 2.97 \text{ \AA}$) and then the AFM3-type ordering (at $d_1 \sim 3.1 \text{ \AA}$) become energetically favorable. However the extended study presented here shows that AFM3-type ordering ceases to be the most stable magnetic state for large lattice expansion, and eventually the collinear FM state is once again the groundstate for $d_1 \gtrsim 3.37 \text{ \AA}$.

In order to experimentally prove the validity of the model, we carefully selected two collinear FM compositions with lattice parameters from the different FM regions of the stability plot in Figure 1. Our choices were CoMnP from the FM(1) regime ($d_1 \sim 2.95 \text{ \AA}$ ²⁰) and CoMnGe ($d_1 \sim 3.4 \text{ \AA}$ ³) from the larger Mn-Mn separation (FM2) zone. Our hypothesis is that progressive substitution of one p element for another in $\text{CoMnGe}_{1-x}\text{P}_x$, without changing the 3d-element concentration, can cause the appearance of metamagnetism in particular compositions of the series. This replacement of large germanium atoms by the much smaller phosphor atoms should result in a shrinkage of lattice. From Figure 1 we expect that the decreasing d_1 separation will lead to the destabilization of FM state in competition with the AFM one at a certain P/Ge ratio. It should then be possible to manipulate the magnetic state of the energetically metastable alloys by changing temperature or applied magnetic field.

In order to identify the key factors that can lead to

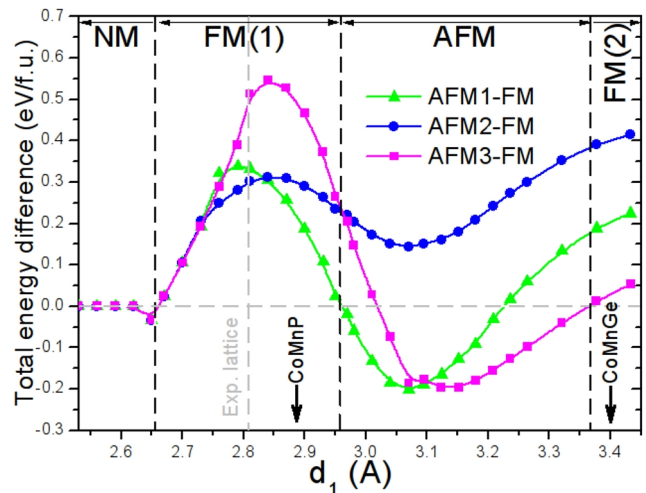


Figure 1: (Color online) Stability of possible collinear magnetic structures, relative to ferromagnetism, within a single unit cell of MnP as a function of d_1 Mn-Mn separation. AFM configurations become stable where $\Delta E_{AFM-FM} < 0$. The vertical dashed line represents the experimental (strain-free, $\varepsilon = 0$) lattice of MnP. We see that the FM state is first destabilised by lattice expansion, and then becomes stable again at large d_1 values: FM(2).

the substantial changes in magnetic groundstate, we first calculate the electronic band structure and magnetic moment of $\text{CoMnGe}_{1-x}\text{P}_x$ alloys with $x=0, 0.25, 0.5, 0.75$ and 1 in a collinear FM state. The calculated magnetic moments are given in Table I. The magnetic moments on Mn ($2.68 \mu_B$) and Co ($0.28 \mu_B$) sites in the CoMnP alloy agrees well with previous calculations based on the KKR method with coherent potential approximation (CPA) by Zach and co-workers²¹. Furthermore, the partial replacement of P by Ge results in a progressive increase of magnetic moment on both 3d elements, leading to an increased M_{Tot} of up to $3.58 \mu_B$ for CoMnGe. A small negative moment induced on the p-block elements is also observed.

The FM total density of electronic states (DoS) of the two end compositions, CoMnP and CoMnGe, are plotted, together with $\text{CoMnP}_{0.5}\text{Ge}_{0.5}$ in Fig. 2. Although the value of total density of states at the Fermi level, $N_{Tot}(E_F) = N_{\downarrow}(E_F) + N_{\uparrow}(E_F)$ exhibits a large change with composition, each total DoS possesses the same features over a large extent of energy range. The main difference is the location of these features, and in particular the location of a pseudogap-like feature in the DoS. Using CoMnP as reference, if the energy scale of the minority DoS is shifted by about $+0.25 \text{ eV}$ for CoMnGe and about -0.3 eV for $\text{CoMnP}_{0.5}\text{Ge}_{0.5}$, not only would the pseudogap fall at E_F but most of the exchange-split DoS peaks of Mn and Co would line up at around the same position. The large $N_{Tot}(E_F)$ in $\text{CoMnP}_{0.5}\text{Ge}_{0.5}$ (Table I) suggests the instability of the collinear FM state in this composition. A possible scenario that stabilizes the

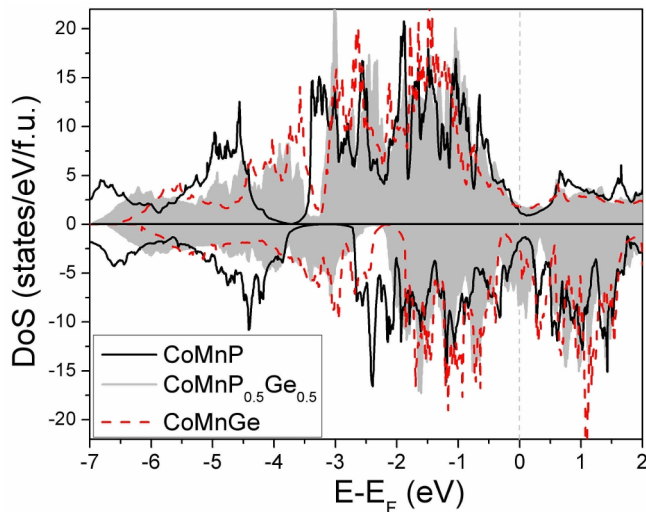


Figure 2: (Color online) Collinear FM total density of states for $\text{CoMnGe}_{1-x}\text{P}_x$ with $x=0, 0.5$ and 1 . The Fermi energy falls into the hybridization gap for both CoMnP and CoMnGe , but shifted for $\text{CoMnP}_{0.5}\text{Ge}_{0.5}$ resulting in a large $N_{Tot}(E_F)$.

x	M_{Mn}	M_{Co}	$M_{Si/Ge}$	M_{Total}	$N_{Tot}(E_F)$
0	3.05	0.6	-0.07	3.58	5.0
0.25	2.83	0.45	-0.06	3.22	10.0
0.5	2.89	0.47	-0.07	3.29	9.5
0.75	2.71	0.33	-0.07	2.97	7.5
1	2.68	0.28	-0.07	2.89	1.7

Table I: Calculated magnetic moments (μ_B) and $N_{Tot}(E_F)$ (states/eV/f.u.) for $\text{CoMnGe}_{1-x}\text{P}_x$.

noncollinear state through the formation of hybridization gap at the Fermi energy is described by Lizárraga et al.⁸. We recently showed the relevance of this mechanism in a noncollinear DFT study on the metamagnet CoMnSi ¹⁰.

In the following sections, we are going to demonstrate the validity of our theoretical prediction of metamagnetism in these Mn-based $Pnma$ alloys through magnetic and structural results on an experimentally synthesized $\text{CoMnGe}_{1-x}\text{P}_x$ series of alloys.

III. EXPERIMENTAL

A. Experimental details

Samples of $\text{CoMnGe}_{1-x}\text{P}_x$ with $x = 0.25, 0.4, 0.5, 0.55, 0.6$ and 0.75 were prepared in a quartz nozzle by an induction melting technique, using Co_2P (99.9%) and Mn_3P_2 (99.9%) master alloys mixed together with high purity Co (99.97%), Mn (99.99%) and Ge (99.9999%) elements in the required proportions. The alloys were cast into a copper mold under protective Ar atmosphere. The ingots were then sealed

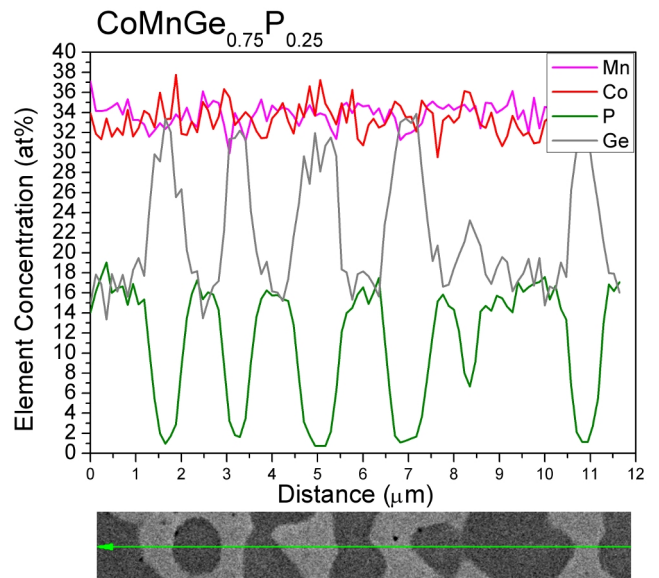


Figure 3: Representative SEM micrograph and corresponding elemental mapping from EDX of $\text{CoMnGe}_{0.75}\text{P}_{0.25}$.

in quartz tube under protective He atmosphere and a homogenization at 1000°C for 24 hours and annealing treatment at 800°C for 72 hours then followed. The samples thus obtained were crushed into fine powder in order to determine their crystal structure using X-ray diffraction (XRD) with $\text{Cu } K\alpha$ radiation. Structural (Rietveld) refinement of the data was carried out using the FULLPROF²² program. A microstructural and compositional analysis was carried out using a Carl Zeiss 1540EsB scanning electron microscope (SEM). Magnetic properties of the samples were studied in a Quantum Design MPMS system.

B. Crystal Structure

Both CoMnGe and CoMnP alloys crystallize in the orthorhombic ($Pnma$, 62) structure in which the elements occupy general $4c$ ($x, \frac{1}{4}, z$) crystallographic positions. XRD analysis of the $\text{CoMn}(\text{Ge},\text{P})$ samples revealed the formation of this orthorhombic structure in all compositions. Furthermore, in the samples with $x = 0.25, 0.4, 0.5$ and 0.75 , extra reflections in the diffraction pattern also appear that can be ascribed to the hexagonal Ni_2In -type ($P6_3/mmc$, 194) lattice structure. The appearance of the higher symmetry hexagonal phase is often observed in similar alloy systems because the orthorhombic structure can be regarded as a distortion from this hexagonal structure and the two structures can be interrelated as follows: $b_{ortho} = a_{hex}$ and $c_{ortho} = \sqrt{3} \times a_{hex}$.

The importance of this latter correlation has been exploited in several Mn-based $Pnma$ systems. In the pseudo-binary $\text{Mn}_{1-x}\text{Fe}_x\text{As}$ alloys the sharp, first order type magnetostructural transforma-

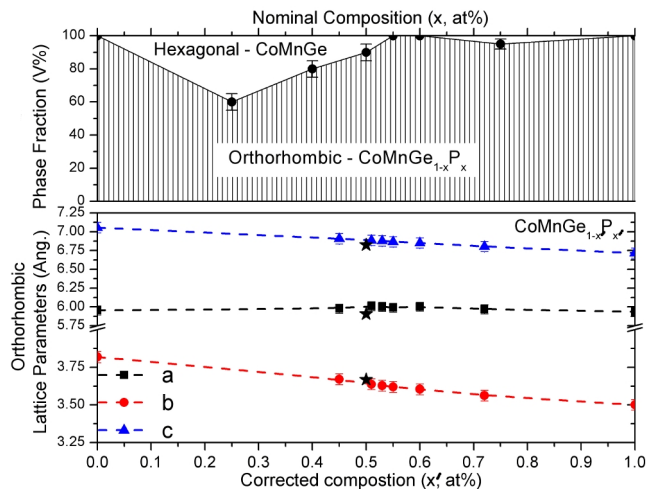


Figure 4: (Color online) Volume fraction of the orthorhombic $\text{CoMnGe}_{1-x}\text{P}_x$ and hexagonal CoMnGe phases as a function of nominal composition (top) and lattice parameters of the main orthorhombic phase as a function of corrected phosphor concentration (bottom). The lattice parameters of CoMnSi , a metamagnet, are added (star symbols) for comparison.

tion (orthorhombic \rightleftharpoons hexagonal)²³ is also accompanied by a “colossal” MCE²⁴. The magnitude of the useful magnetic entropy change is, however, now strongly contested²⁵. A similar magnetostructural transition in CoMnGe -based ternary compositions was reported by Kanomata and co-workers who observed a large, $\sim 5.3\%$, volume change^{26,27}. Theoretical calculations also revealed that the Co vacancy-induced phase transformation is due to a high moment to low moment magnetic transition accompanied by a large magnetovolume effect originating from the change of the coupling distance between the principal magnetic atoms²⁸. As an extension of this study, both Hamer¹⁶ and Trung^{17,18} recently demonstrated that the transitions can be fine-tuned by pseudo-ternary additives (Sn, B or Cr elements) around room temperature for an enhanced magnetocaloric effect. The appearance of the hexagonal structure at room temperature in our samples can therefore be understood as a first order transformation from the low temperature orthorhombic structure to a high temperature hexagonal one.

In order to clarify the composition of the hexagonal phase, a representative secondary electron (SE) SEM micrograph was taken from the $\text{CoMnGe}_{0.75}\text{P}_{0.25}$ alloy and is shown in Fig. 3a. The two different structural regions are identified in accordance with the XRD results. EDX elemental mapping revealed that the two phases have substantially different atomic compositions. Our investigations show that the orthorhombic phase is poor in Ge (and consequently enriched in P) whereas the second phase is enriched in Ge and is therefore close in composition to stoichiometric CoMnGe . An atomic composition profile taken along the direction of the arrow indicated in Fig. 3b shows quantitatively the compositional dif-

ference between the two structures. These findings are direct evidence for a compositional phase separation of the quaternary alloy rather than for a second-order type transformation of the single quaternary composition with temperature.

The results of the quantitative Rietveld analysis in Fig. 4 (top) reveal the formation of single phase orthorhombic structures in the alloys rich in P ($x > 0.5$). Fig. 4 (bottom) summarizes the lattice parameter of the orthorhombic structure as a function P content. (The composition values (x') given in the lower figure are corrected based on the quantitative analysis.) The b and c lattice constants show decrease continuously with Ge addition while the a parameter stays nearly constant and until the lattice parameters with $x \sim 0.5$ become close to those of the metamagnet CoMnSi .

In the next section, we will demonstrate the occurrence of metamagnetism in these Mn-based alloys that have appropriately designed lattice parameters.

C. Magnetic properties

As we demonstrated in Sec. III B, the lattice parameters of the $\text{CoMnP}_{1-x}\text{Ge}_x$ alloy can be tuned towards those of the CoMnSi metamagnet. In the present section, we will show that this structural engineering allows us to prepare metamagnetic quaternaries, even though the end alloys (CoMnP and CoMnGe) are ordinary ferromagnets. Based on the a , b and c lattice parameters of the $\text{CoMnGe}_{1-x}\text{P}_x$ alloys, one would expect progressive change from collinear ferromagnetism to non-collinear anti-ferromagnetism with the replacement of P by Ge in the system. At around $x \sim 0.5$ the structure should resemble that of the CoMnSi metamagnet and once the composition is on the P-rich end of the series, ferromagnetism should re-appear. Indeed, we have found this scenario to be fulfilled; however the structural phase separation into a ternary CoMnGe and a residual $\text{CoMn}(\text{Ge},\text{P})$ phase in compositions that are rich in Ge hinders a simple interpretation.

The composition dependence of magnetisation loops taken at 10 K is shown in Fig. 5. Metamagnetism is most visible in the single phase compositions with $x = 0.55$ and 0.6. In these samples, the initial magnetisation varies almost linearly with applied field below the inflection point that occurs at a critical field value. Although this critical behaviour is also visible in all compositions with $x \leq 0.6$, the increasing volume of ferromagnetic CoMnGe phase at low x suppresses the sharpness of the upturn in magnetisation. A distinct shift of the peak of $\frac{\partial M}{\partial H}$, seen in Fig. 5b shows that the critical field decreases sharply as more Ge is replaced by P (towards small x).

The composition dependence of the critical field in a field of 1 Tesla is shown in Fig. 6 and is consistent with the magnetisation loops collected at 10 K. The lower the critical field that is observed at 10 K (Fig. 5), the lower the critical temperature is at which the 1 T applied mag-

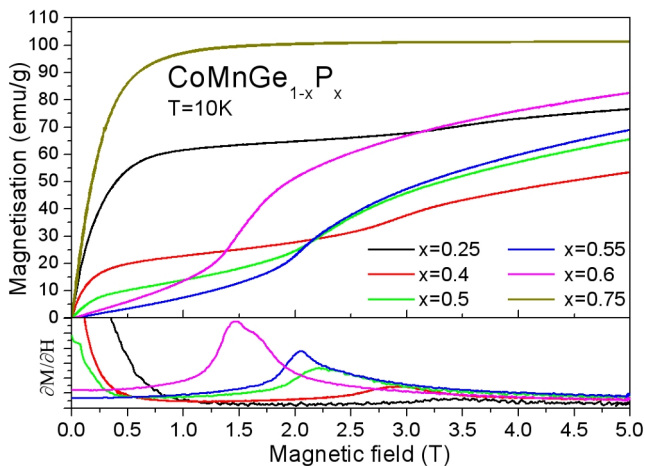


Figure 5: (Color online) Magnetisation loops of $\text{CoMnGe}_{1-x}\text{P}_x$ at 10K.

netic field is sufficiently large to bring the sample to the high magnetic state. A strong dependence of the metamagnetic transition temperature on crystal structure is evident from this Figure, when compared with Fig. 4. Although samples with $x \leq 0.5$ contain a minor second phase, they all show a characteristic increase in the magnetisation as a function of temperature, indicative of native metamagnetism. In the high Ge (low x) side of the series, with $x=0.25$, although the substantial ferromagnetic volume (from the CoMnGe phase) largely suppresses the metamagnetic transition, it still appears at around room temperature (RT).

As the samples become richer in phosphor, the critical temperature decreases sharply from $\sim 300\text{K}$ to $\sim 80\text{K}$ and it eventually disappears for $x=0.75$. The highest magnetisation values in a 1 T applied field show an increase with x (except for $x=0.25$) as the result of a balance of several effects. Firstly, it is easily foreseeable that at lower transition temperatures ferromagnetic configurations will exhibit larger overall net moments compared to those of the higher temperature ones. Secondly, the presence of the hexagonal CoMnGe lifts the low temperature “baseline” of magnetisation in Fig. 6.

IV. SUMMARY AND CONCLUSIONS

Using DFT calculations based on a “prototype” binary MnP composition, we have investigated the occurrence of AFM and FM states in Mn-based orthorhombic ($Pnma$, 62) alloys. As the result of isotropic expansion, the FM(1) ground state is no longer stable but instead AFM coupling of the spins on the Mn atoms is predicted above $d_1 \gtrsim 2.95 \text{ \AA}$ ¹¹. In this work, we have extended our theoretical investigation to higher hydrostatic expansions and found the re-occurrence of ferromagnetism (FM2) at large Mn-Mn separations over $d_1 \gtrsim 3.37 \text{ \AA}$ that also explains the collinear ferromagnetism in CoMnGe with

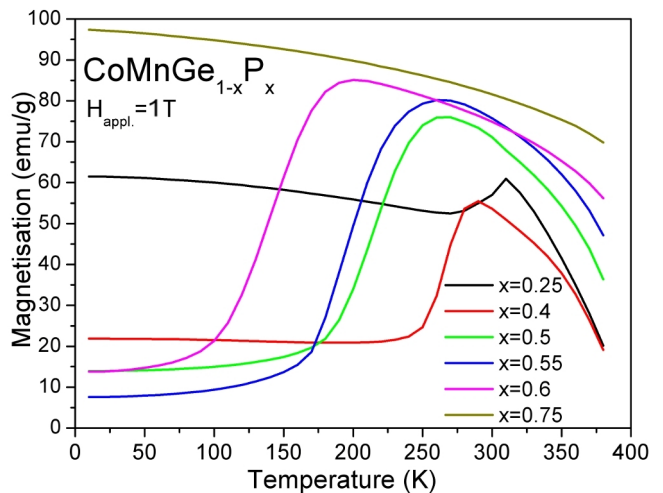


Figure 6: (Color online) Iso-field magnetisation of $\text{CoMnGe}_{1-x}\text{P}_x$ as a function of temperature, measured in a 1 Tesla applied field. We observe metamagnetism in almost all samples, and a sharp change in the metamagnetic critical temperature with composition in the range $x=0.4$ to 0.6.

$$d_1 = 3.4 \text{ \AA}.$$

Based solely on the deduced magnetic stability plot (Fig. 1), we designed a series of pseudo-ternary CoMn -based alloys in order to experimentally prove the validity of our theoretical concept. Taking two collinear FM ternaries: one, CoMnP with a low d_1 from the FM1 region ; the other, CoMnGe with a high d_1 from the FM2 region we attempted to drive the alloy magnetism towards the metamagnetic/AFM zone by careful structural design.

The experimental investigation of $\text{CoMnGe}_{1-x}\text{P}_x$ has indeed revealed an AFM ground state for compositions $x \approx 0.5$. The appearance of a magnetic field- and temperature-dependent metamagnetic transition in several samples also suggests the existence of complex non-collinear spin structure in most of them , and in particular in the range $x=0.4$ to 0.6. The large predicted $N_{Tot}(E_F)$ for $x = 0.5$ (in Sec. II) in a hypothetical FM state is because of a shift in the energy of the hybridisation-derived pseudogap as the lattice parameters expand upon Ge substitution for phosphor.

Although the complex magnetic spin structure of these new samples is to be determined, the system is an example of the stabilization of non-collinear magnetism through the formation of hybridization gap at the Fermi energy as described by Lizárraga et al.⁸ and as recently found in the ternary CoMnSi ¹⁰. The Mn-containing $Pnma$ structure is extremely versatile with regard to elemental substitution. The above demonstration of a structurally-directed tuning of magnetic properties therefore provides a potential direction for future tailoring of metamagnetic phase transitions towards their use in applications such as those that rely on the magnetocaloric effect.

Acknowledgments

Z. G. is grateful for the invitation and financial support of NIMS through the Open Research Institute Program. K.G.S. acknowledges financial support from The Royal Society. Furthermore, the authors thank H. S. Amin for his assistance in the SEM sample preparation and analy-

sis. The research leading to these results has received funding from the European Community's 7th Framework Programme under grant agreement No. 214864 ("SSEEC"). Computing resources provided by Darwin HPC and Camgrid facilities at The University of Cambridge and the HPC Service at Imperial College London are gratefully acknowledged.

-
- ¹ T. Nagamiya, *Solid State Phys.* **20**, 305 (1967).
² A. Kallel, H. Boller, and E. Bertaut, *J. Phys. Chem. Solids* **35**, 1139 (1974), ISSN 0022-3697.
³ S. Nizioł, A. Bombik, W. Bazela, A. Szytuła, and D. Fruchart, *J. Magn. Magn. Mater.* **27**, 281 (1982).
⁴ T. Eriksson, L. Bergqvist, T. Burkert, S. Felton, R. Tellgren, P. Nordblad, O. Eriksson, and Y. Andersson, *Phys. Rev. B* **71**, 174420 (2005).
⁵ S. Nizioł, H. Binczycka, A. Szytuła, J. Todorovic, R. Fruchart, J. Senateur, and D. Fruchart, *phys. stat. sol. (a)* **45**, 591 (1978).
⁶ L. Dobrzynski and A. Andresen, *J. Magn. Magn. Mater.* **82**, 67 (1989), ISSN 0304-8853.
⁷ R. J. Elliott and F. A. Wedgwood, *Proceedings of the Physical Society* **81**, 846 (1963).
⁸ R. Lizárraga, L. Nordström, L. Bergqvist, A. Bergman, E. Sjöstedt, P. Mohn, and O. Eriksson, *Phys. Rev. Lett.* **93**, 107205 (2004).
⁹ K. G. Sandeman, R. Daou, S. Özcan, J. Durrell, N. Mathur, and D. Fray, *Phys. Rev. B* **74**, 224436 (2006).
¹⁰ A. Barcza, Z. Gercsi, K. S. Knight, and K. G. Sandeman, *Phys. Rev. Lett.* **104**, 247202 (2010).
¹¹ Z. Gercsi and K. G. Sandeman, *Phys. Rev. B* **81**, 224426 (2010).
¹² H. Fjellvåg, A. Andresen, and K. Bärner, *Journal of Magnetism and Magnetic Materials* **46**, 29 (1984).
¹³ B. Sredniawa, R. Zach, P. Fornal, R. Duraj, A. Bombik, J. Tobola, S. Kaprzyk, S. Nizioł, D. Fruchart, M. Bacmann, et al., *J. Alloys Compounds* **317-318**, 266 (2001).
¹⁴ W. Bazela, A. Szytuła, J. Todorovic, and A. Zieba, *phys. stat. sol.* **64**, 367 (1981).
¹⁵ V. Johnson, *Inorganic Chemistry* **14**, 1117 (1975).
¹⁶ J. Hamer, R. Daou, S. Ozcan, N. Mathur, D. Fray, and K. G. Sandeman, *J. Magn. Magn. Mat.* **321**, 3535 (2009).
¹⁷ N. T. Trung, V. Biharie, L. Zhang, L. Caron, K. H. J. Buschow, and E. Bruck, *Applied Physics Letters* **96**, 162507 (pages 3) (2010).
¹⁸ N. T. Trung, L. Zhang, L. Caron, K. H. J. Buschow, and E. Bruck, *Applied Physics Letters* **96**, 172504 (pages 3) (2010).
¹⁹ G. Kresse and J. Furthmuller, *Phys. Rev. B* **54**, 11169 (1996).
²⁰ D. Fruchart, M. Backmann, and P. Chaudouet, *Acta Crystallographica Section B* **36**, 2759 (1980).
²¹ R. Zach, J. Tobola, B. Sredniawa, S. Kaprzyk, M. Guillot, D. Fruchart, and P. Wolfers, *J. Phys.: Condens. Matter* **19**, 376201 (2007).
²² J. Rodríguez-Carvajal, *Physica B: Condensed Matter* **192**, 55 (1993), ISSN 0921-4526.
²³ H. Fjellvåg, A. Kjekshus, A. F. Andresen, and A. Zieba, *Journal of Magnetism and Magnetic Materials* **73**, 318 (1988), ISSN 0304-8853.
²⁴ A. de Campos, D. Rocco, A. Magnus, G. Carvalho, L. Caron, A. Coelho, S. Gama, L. da Silva, F. Gandra, A. dos Santos, et al., *Nature Materials* **5**, 802 (2006).
²⁵ M. Balli, D. Fruchart, D. Gignoux, and R. Zach, *Applied Physics Letters* **95**, 072509 (pages 3) (2009).
²⁶ T. Kanomata, H. Ishigaki, T. Suzuki, H. Yoshida, S. Abe, and T. Kaneko, *Journal of Magnetism and Magnetic Materials* **140-144**, 131 (1995), ISSN 0304-8853, international Conference on Magnetism.
²⁷ K. Koyama, M. Sakai, T. Kanomata, and K. Watanabe, *Japanese Journal of Applied Physics* **43**, 8036 (2004).
²⁸ J.-T. Wang, D.-S. Wang, C. Chen, O. Nashima, T. Kanomata, H. Mizuseki, and Y. Kawazoe, *Applied Physics Letters* **89**, 262504 (pages 3) (2006).